nature geoscience

ARTICLES

https://doi.org/10.1038/s41561-019-0335-5

Atmospheric transport and deposition of microplastics in a remote mountain catchment

Steve Allen[1,2,5], Deonie Allen[1,5*], Vernon R. Phoenix[2], Gaël Le Roux[1], Pilar Durántez Jiménez[1], Anaëlle Simonneau[3], Stéphane Binet[1,3] and Didier Galop[4]

Plastic litter is an ever-increasing global issue and one of this generation's key environmental challenges. Microplastics have reached oceans via river transport on a global scale. With the exception of two megacities, Paris (France) and Dongguan (China), there is a lack of information on atmospheric microplastic deposition or transport. Here we present the observations of atmospheric microplastic deposition in a remote, pristine mountain catchment (French Pyrenees). We analysed samples, taken over five months, that represent atmospheric wet and dry deposition and identified fibres up to ~750 µm long and fragments ≤300 µm as microplastics. We document relative daily counts of 249 fragments, 73 films and 44 fibres per square metre that deposited on the catchment. An air mass trajectory analysis shows microplastic transport through the atmosphere over a distance of up to 95 km. We suggest that microplastics can reach and affect remote, sparsely inhabited areas through atmospheric transport.

Plastic industry experts estimate the global manufacture of 335 million tonnes (Mt) of plastic in 2016[1]. Of the 335 Mt worldwide, 60 Mt was produced in Europe, of which ~40% is packaging (short term or single use). In 2016, however, 27.1 Mt was recovered as waste for recycling, energy recovery (burning) or placed in landfill[2,3]. Some plastics remain in service for up to 50 years, which helps explain some of the 32.9 Mt discrepancy in the plastics mass balance. Although plastic is recognized to biodegrade very slowly, degradation to micro (5 mm to 1 µm) and nanoplastics (<1 µm) does occur[4,5]. Thus, plastic waste can start as macroplastic pieces (bottles, packaging and so on) and over time degrades to microplastic (MP) particles or smaller. Mattsson et al.[6] estimate that 10% of created plastics enter the ocean annually, which accounts for a portion of the 32.9 Mt plastic waste. However, this highlights questions on the fate of the remaining plastic. Large amounts of macroplastic waste would be noticed in the terrestrial environment, but if this waste degraded to microsized particles it could evade easy detection. Recent studies identified MPs on alpine river floodplains[7] and lake sediment[8], which illustrates the terrestrial MP occurrence, and in megacites as aerosol pollution[9–12]. The recent research on atmospheric fallout in Paris[9–11] and Dongguan[12] suggests an atmospheric MP conveyance and corresponding deposition. Soil, sediment and lake samples provide an informative terrain-based analysis of plastic[7,13–16] occurrence; however, the determination of atmospheric MPs beyond intra-city deposition requires source-specific and remote atmospheric sampling.

This research provides unequivocal evidence of the direct atmospheric fallout of MPs in a remote area of the Pyrenees mountains. The Pyrenees mountainous regions are anecdotally considered pristine wilderness due to the limited development, difficulty of human access and distance from major populations or industrial centres. The study site is located at the Bernadouze meteorological station[17], 42° 48′ 14.6″ N, 1° 25′ 06.8″ E and 1,425 m above sea level, within the Vicdessos catchment and mid-Pyrenees mountains in the south-west of France (Supplementary Note 1). The local vicinity is sparsely populated, without industrial, commercial or large agricultural activities, and is primarily used for recreational activities (hiking, skiing, environmental education and scientific research). The closest local residential area is a village ~6 km to the southeast (Vicdessos village, population ~540; ref. [18]) with a moderately sized town located ~25 km to the northeast (Foix, population ~9,720; ref. [18]).

The presented research considers five months of atmospheric deposition collected from the field site. Five samples of total atmospheric deposition (wet and dry) from two separate monitoring devices were analysed to identify whether MPs are present in the remote mountain catchment. Regular (monthly) sampling campaigns were proposed; however, weather conditions restricted the site access, which resulted in irregular monitoring intervals (Methods and Supplementary Table 1). The objective of observing the case study atmospheric deposition was to identify (1) if MPs are present in the atmospheric fallout in this remote mountainous location and (2) if MPs are present, in what quantity, size, shape and plastic type do they occur? The purpose of this study was to take steps towards discovering the extent of the MP atmospheric deposition in remote terrestrial locations.

MP particles in the remote mountain catchment

MP fragments, fibres and films were found and confirmed (through visual microscopy inspection and micro-Raman analysis[19]) in all the atmospheric deposition samples collected from the field site. This illustrates that for this location there is an atmospheric MP presence. The atmospheric MP deposition captured in the collectors are presented in Fig. 1.

Details of the local meteorological conditions recorded at the sampling site are provided in Supplementary Table 1 in conjunction with the normalized MP counts per day (MP m^{-2} d^{-1}). The meteorological record illustrates a lower relative precipitation and fewer storms (rain or snow) in November compared to the following months. The relative snowfall increased over the monitoring period, whereas rainfall was greatest in the January. Monthly average wind

[1]EcoLab (Laboratoire Ecologie Fonctionnelle et Environnement), ENSAT, UMR-CNRS 5245, Castanet Tolosan, France. [2]Department of Civil and Environmental Engineering, University of Strathclyde, Glasgow, UK. [3]ISTO, CNRS UMR 7327, Université d'Orléans, BRGM, Orléans, France. [4]GEODE, UMR-CNRS 5602, Université Toulouse Jean Jaurès, Toulouse, France. [5]These authors contributed equally: S. Allen, D. Allen. *e-mail: deonie.allen@ensat.fr

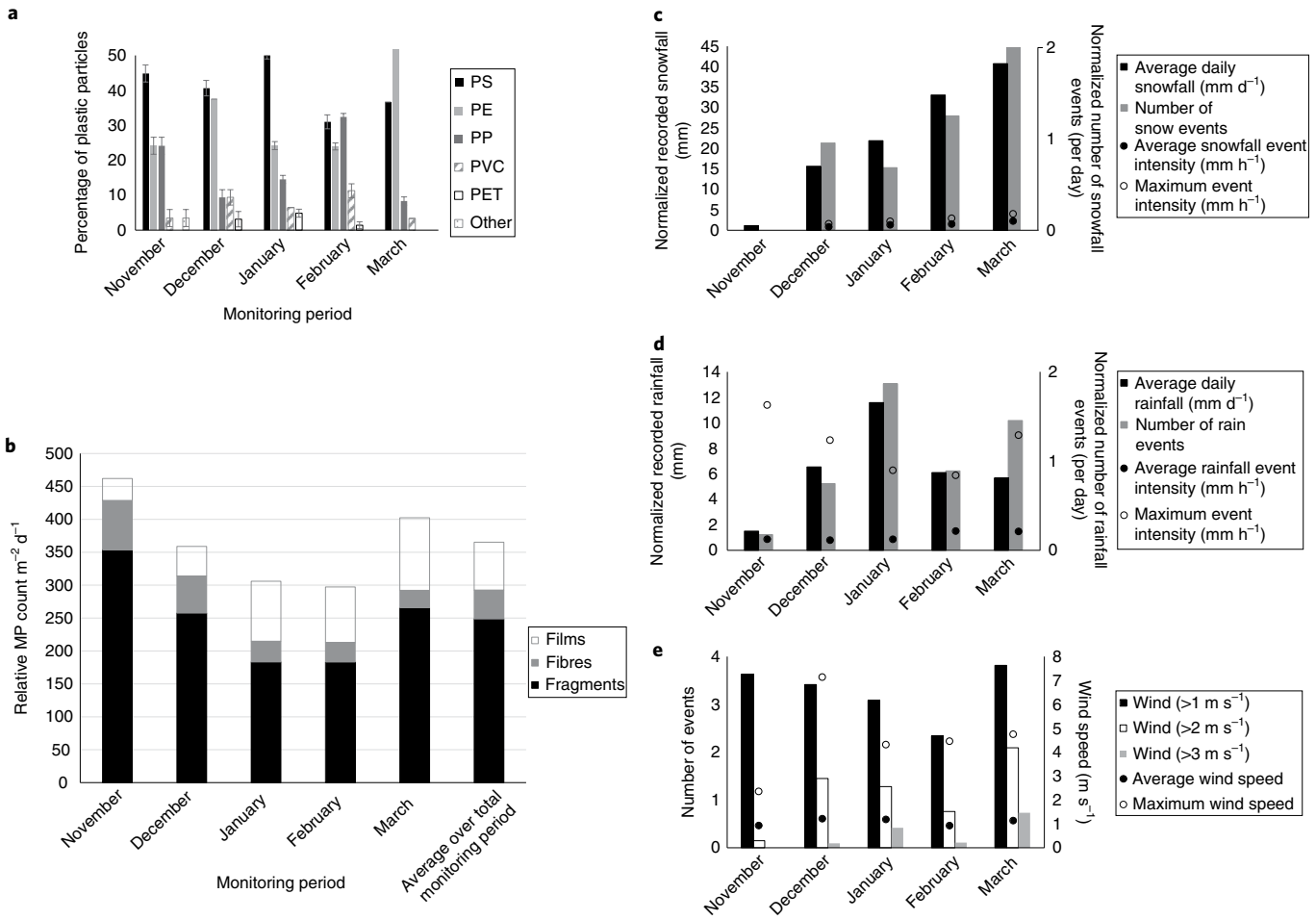

Fig. 1 | Atmospheric MP deposition captured in the collectors. a–e, MP type (**a**), MP occurence (**b**) and recorded local snowfall (**c**), rainfall (**d**) and wind speed and wind events (**e**) for the monitored period. Supplementary Information comments on the fragment, fibre and film ratio. The types of plastics found in the atmospheric fallout are derived from Raman spectroscopy analysis, SpectraGryph spectral analysis software and libraries[38–42]. The plastic types are presented as abbreviations: PS, polystyrene; PE, polyethylene; PP, polypropylene; PVC, polyvinyl chloride; PET, polyethylene terephthalate; other, uncharacterized.

speed fluctuated around $1.1 \pm 0.6\,m\,s^{-1}$ with a maximum recorded wind speed of $7.1\,m\,s^{-1}$ in December. December–March show wind speeds $>4\,m\,s^{-1}$ and the greatest relative number of wind events ($>2\,m\,s^{-1}$ and $>3\,m\,s^{-1}$) occurred in March. The numbers of $>1\,m\,s^{-1}$ events were greatest in November and March, declining to the lowest frequency in February.

Field sample MP counts illustrate an average daily particle deposition of $365\,m^{-2}\,d^{-1}$ (± 69, s.d.). Sample MP counts were normalized to represent the daily atmospheric deposition as site-access limitations resulted in inconsistent monitoring durations (November extended 12 days, December 19 days, January and March 34 days and February 41 days).

Both rainfall and snowfall show moderate to strong significant correlations with MP count in the original data set ($r \geq 0.8$, $p < 0.05$) and to the monitoring duration (days) (Supplementary Note 2). The normalized data set presents a positive correlation to the frequency of wind speeds >1 m/s (light air-strong wind movement) ($r > 0.8$, $p < 0.05$) suggesting MP transport and deposition may be influenced by wind movement. The maximum rainfall intensity also presents a strong positive correlation ($r > 0.9$, $p < 0.05$) suggesting that individual events and the intensity of events may influence atmospheric MP deposition (scavenging)[20]. Although it is acknowledged that the data set is limited, the number of snowfall events also shows a positive correlation with normalized MP deposition ($r \geq 0.6$, $p < 0.05$). The duration (average and maximum) of both rainfall and snowfall events illustrate negative correlations with MP deposition ($r \leq -0.6$) suggesting event occurrence and intensity rather than duration may positively influence MP deposition[21,22]. Despite long durations (≤41 days) represented by the samples, this preliminary data set suggests that rain, snow and wind events may be drivers in MP deposition at this site. This supports the suggestion by Dris et al.[10] that precipitation events may be a positive driver in atmospheric MP fallout.

The samples collected for the January–March monitoring period contained a visible quantity of orange quartz-like fine dust. This dust presented the size (median grain size ~8 µm), colour and indicative chemical signature descriptive of Saharan dust[23,24] (Supplementary Data gives further details). The fine dust and other particulate matter that potentially include some MP particles are possibly Saharan-, North African- or Iberian-sourced material (or potentially sourced along this trajectory)[25]. For example, the long-range transport of dust was shown by van der Does et al.[26], who found ultragiant particles (<400 µm) that travelled up to 3,500 km trans-oceanically. The distance MP particles can travel is currently unknown and further event-based research is needed to identify the source and transport vectors of atmospheric MP particles.

Characteristics of MP particles

The characterization was completed following the identification guide presented by Hidalgo-Ruz et al.[27] and Norén[28] in conjunction

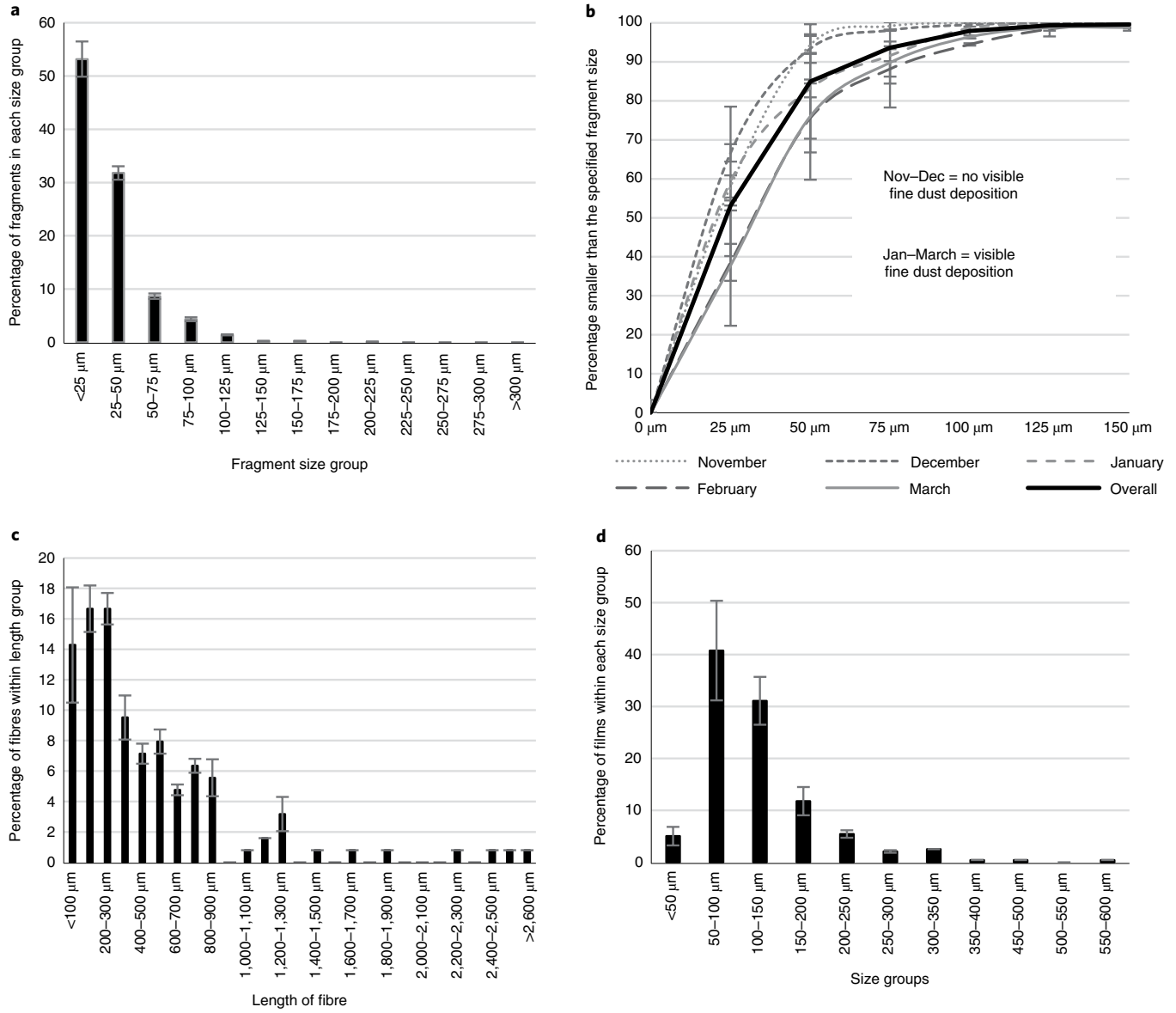

Fig. 2 | Deposited MP characterization. a,**b**, Particle size distribution for the MP particles in the atmospheric deposition samples and for the monitoring period. **c**, Range and predominant fibre lengths. **d**, Average diameter of the films collected in the collectors during the monitoring periods.

with micro-Raman analysis. The MP particle size or length was defined using the particle characterization and count functions in ImageJ/Fiji[29] following the method presented by Erni-Cassola et al.[30]. The overall particle sizes for the MPs are presented in Fig. 2, with the individual monitoring period sample fragment sizes illustrated in Fig. 2b.

The majority of environmental MP studies that have considered particle size distribution (PSD) illustrate an increasing trend in the number of finer fragments (a significantly greater number of MP fragments with a smaller particle size)[9,12,31]. The remote atmospheric deposition samples illustrate the majority of identified MP fragments to be ≤50 µm and the overall fragment size trend follows previous MP particle size trends. When considered relative to the monitoring period (Fig. 2b), there is a slight shift in the PSD curve that appears to correspond to the fine dust deposition. Samples with no visible quantity of fine dust (November and December) show a greater quantity of smaller fragments. The fine dust-laden samples show a small increase in primary fragment size (February–March). Note that for the fine dust sample periods there are a greater number of elevated wind periods (wind events >2 m s^{-1}), higher maximum recorded wind speeds and interspersed periods of calm (wind speed 0.5 m s^{-1}) that may assist in the conveyance and deposition of the MP fragments.

The length of plastic fibres found in the atmospheric fallout samples (Fig. 2c) suggests predominant fibre lengths of 100–200 µm and 200–300 µm. Cai et al.[12] found the majority of fibres in Dongguan to be 200–700 µm in length with fibres of ≥4,200 µm (longest fibre), whereas Dris et al.[10,11] primarily found fibres of 200–600 µm, with the longest recorded fibre of ~5,000 µm. When the scale for the fibre length analysis is modified to fit previous studies, the fibre lengths of the Pyrenees site fall predominantly between 200 and 700 µm (47%) (Cai et al.[12] present ~30% in this predominant category) and 50–200 µm (30%) (Dris et al.[10,11]] illustrate a higher predominant fibre length of 400–600 µm (23%)). The longest fibre identified as a plastic fibre in this mountain field study was 3,000 µm. Film size was not specifically evaluated in previous atmospheric MP analysis, so limited comparative information is currently available. Films can be very thin and flat, and therefore provide a greater surface area

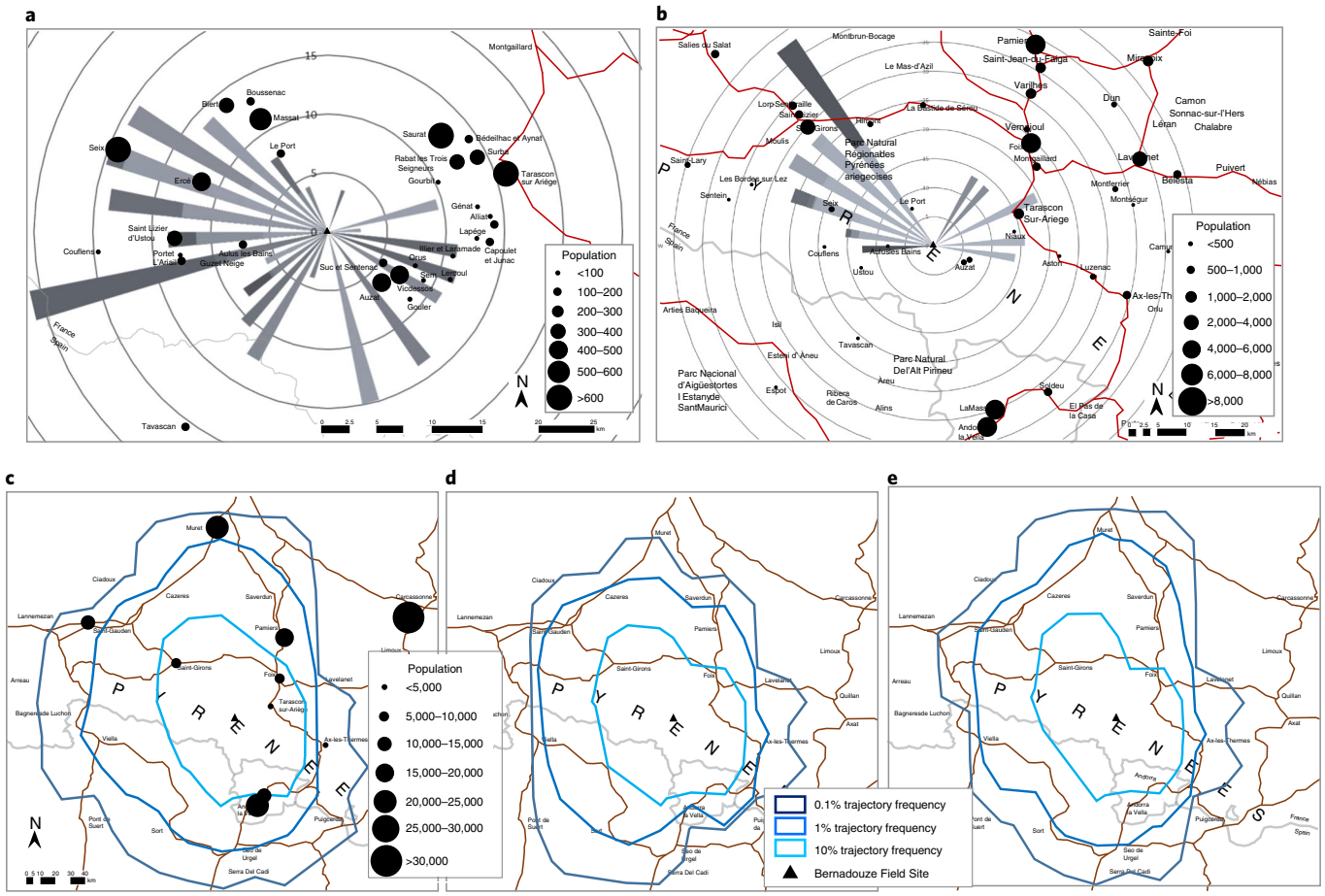

Fig. 3 | MP transport trajectories relative to the recorded meteorology (simplistic MP settling velocity trajectory calculation) and HYSPLIT4 back-trajectory modelling. a, Rain ($n=165$) and snow ($n=186$) event trajectories calculated from the maximum recorded wind speed and wind direction of each storm. **b**, Trajectories of wind events >2 m s^{-1} ($n=197$). **c**–**e**, HYSPLIT4 back-trajectory model results for each individual wind event >2 m s^{-1} (**c**), rainfall event (**d**) and snowfall event (**e**). The results are collated and presented as trajectory frequency graphs. The wind direction data are presented with reference to local populated areas to provide a spatial reference.

for atmospheric conveyance relative to fragments of the same mass (Fig. 2a,d). Within this mountain field study, the predominant film diameter was 50–200 µm, larger than the predominant fragment size.

Raman spectroscopic analysis provides a verification of fragments, fibres and films as plastic[31] and the characterization of plastic type (Fig. 1). The predominant plastic found in the samples is polystyrene (PS) (as fragments), closely followed by polyethylene (PE). PS and PE are used in many single-use plastic items and in packaging material. Approximately 40% of plastic demand is for plastic packaging and PS or PE products[32]. PS and PE are recyclable products; however, in 2016 the European recycling rate was ~31% overall (all plastics) and ~41% for plastic packaging[32] with 3.4 Mt of plastic packaging disposed in European Union landfill. PE has a low density compared to that of other plastics, 0.92–0.97 g cm^{-3} (ref. [27]) and is a common film plastic (such as in plastic bags)[33]. PS is a common packaging material with thermal insulating features and the ability to provide both strong and light-weight plastic products. PS has a higher density than PE, 0.96–1.1 g cm^{-3} (ref. [27]); however, it is often used in a foam form for packaging, insulation and protection, which results in a significantly lowered density. Polypropylene (PP) comprises 18% of the identified plastic particles (fibres are primarily PP and polyethylene terephthalate (PET)). PP is used in packaging, textiles and reusable products. It is the least dense of all plastics (0.9–0.91 g cm^{-3} (ref. [27]) and, due to its use in the textile industry, is constructed as fibres as well as objects or films.

The composition of plastic fallout varied over the monitoring period. The initial correlation analysis did not indicate any strong, significant correlations between plastic type and the recorded meteorology (rainfall, snowfall, wind speed or wind events). The complexity of the plastic composition may be due to the source of plastic particles (and therefore wind direction and strength), the occurrence of storm events and the duration of calm days relative to event occurrence. The initial consideration of atmospheric MP fallout and meteorological conditions does not suggest a simple meteorological mechanism that drives specific or preferential plastic deposition at this field site, but does illustrate PS, PE and PP to be the three greatest contributors to the atmospheric fallout at this location.

Remote MP deposition compared to megacity MPs

The MP deposition recorded at this field site equates to an average daily MP deposition of 365 m^{-2} d^{-1} (±69, particles ≥5 µm). Previous atmospheric fallout monitoring[11,12] undertaken in high-density urban areas identified a daily fallout of 110 ± 96 and 53 ± 38 particles m^{-2} d^{-1} (Paris)[10,34] and 228 ± 43 particles m^{-2} d^{-1} (36 MP particles m^{-2} d^{-1} confirmed) (Dongguan)[12]. Both the Paris and Dongguan studies counted and analysed particles ≥100 µm, ≥50 µm and ≥200 µm respectively. If only ≥200 µm particles are counted in the remote mountain field samples, this equates to 40 ± 20 particles m^{-2} d^{-1}, 70% as fibres. The Pyrenees field site MP deposition is

comparable to the reported megacity atmospheric MP deposition, despite the remote and mountainous location of notable distance from urban city development or infrastructure.

Both the Paris and Dongguan studies primarily focused on MP fibres. If only fibres are considered, the relative daily MP fibre deposition is 36 ± 18 fibres $m^{-2} d^{-1}$ ≥100 µm, or 28 ± 13 fibres $m^{-2} d^{-1}$ ≥200 µm. This is lower than but comparable to megacity average MP counts. The fibre count for the Pyrenean site for MP fibres ≥100 µm ranges from 22 to 62 fibres $m^{-2} d^{-1}$. The Paris megacity study includes periods of lower MP deposition than seen in this field study (Paris MP deposition range is 2–355 MP $m^{-2} d^{-1}$), potentially due to the greater precipitation quantity and frequency at the Pyrenees field site compared to the Paris study period. It is noted that, in concurrence with the Paris and Dongguan findings, there appears to be no direct correlation between MP deposition and average daily rainfall, but the occurrence of precipitation events (rain or snow) and their specific characteristics, intensity and frequency may be drivers in atmospheric fallout.

The MP sample composition of the Paris and Dongguan studies differs in plastic type as well as shape to the findings of this study. PS and PE form a large portion of the plastic type found in the Pyrenees field site. The majority of PS particles were fragments, whereas most fibres were PET or PP. The Pyrenees field study, similar to the Swiss floodplain findings[7], found the MP composition to differ from those of the city atmospheric findings[11,12]. Although acknowledging the different environmental compartments, there also several oceanic-focused studies that identified high counts of PS alongside PE and PP[35]. Emerging research on the degradation rate of plastics by type suggests that PS, especially expanded PS, is highly sensitive to mechanical and ultraviolet degradation (when compared to PP and PE)[4]. Expanded PS MPs may be less dense and more easily entrained (therefore transported), which may help explain the findings at this field site. The composition of plastic waste lost to the environment (not recycled or recovered) is not well documented and this, combined with limited knowledge on degradation rates, makes it difficult to quantify and characterize the plastic waste type, shape and size that 'escape' to the environment.

Remote atmospheric MP source and transport analysis

Atmospheric MP source and transport analyses are new to MP research. Local to regional transport has been considered for this field site using two methods, a simple MP settling calculation and short-duration HYbrid Single Particle Lagrangian Integrated Trajectory (version 4, HYSPLIT4) back-trajectory modelling (Methods). Back-trajectory duration is defined as ~2 h (0.1 m s^{-1} settling velocity[36] for 600 m above ground level (a.g.l.). Pyrenean planetary boundary layer depth[37]) and each individual wind (>2 m s^{-1}), rain and snow event were analysed to provide a spatial context for the local MP transport. The simple MP settling calculations (Methods equation (4)), using MP settling velocity, event wind speed and direction and planetary boundary layer depth[37], provide basic, linear back-trajectories for MP deposited at the field site due to the initial entrainment or uplift and horizontal (wind) conveyance (without further mechanical or convective lift). The MP source area or zone of influence defined by this method extends for 28 km northwest to southwest, along the sparsely populated Aulus-les-Bains, Ercé and Massat valleys, over the Guzet-Neige ski fields and south-east along the Vicdessos valley (Fig. 3a,b). Wind events >2 m s^{-1} illustrate a local MP source area across Aulus-les-Bains and the Saint-Girons valleys (42 km to the northwest) and 20 km to the northeast over Tarascon-sur-Ariège (village populations <6,000).

HYSPLIT4 back-trajectory modelling allows individual event air parcels to be back-traced to illustrate the air parcel trajectory. Using the calculated back-trajectory duration (Methods), models for individual rain, snow and wind events were created and collated to provide event-based back-trajectory frequency maps (Fig. 3c–e). These short-duration back-trajectories include localized updraft, convective mixing and advection, and thus extend the MP transport trajectories and the source area 60 km to the east, 75 km to the west and south, and 95 km to the north of the site. HYSPLIT4 MP source areas extend into western Andorra (Andorra le Vella, population ~22,250), the Spanish Pyrenees, the Saint Gaudens valley and across Foix to Muret (population~24,975). However, like the MP settling calculations, they still fall short of the more densely populated and industrialized areas likely to be significant MP emission sources (Toulouse (population ~466,000), Barcelona (population 1.6 million), Zaragoza (population ~661,000)). This data set does not support long-range transport analysis due to the sampling timestep; however, MP emissions are unlikely to be limited to local sources (<100 km) due to the low local population density.

Evidence of remote atmospheric deposition and transport

This study reports the atmospheric deposition of MPs in a remote Pyrenean mountain location. The research shows the monitored site received large numbers of MP particles (365 $m^{-2} d^{-1}$) in atmospheric deposition collectors over the winter period of 2017–2018. The presented research illustrates the presence of MPs in a non-urban atmospheric fallout. Analysis for this single site suggests a tentative but possibly important link between precipitation (rain and/or snow), wind speed and wind direction to the MP deposition. Initial local MP trajectory assessment indicates an MP source area that extends to 95 km from the site, reaching several towns (populations <25,000) but not the city MP emission sources, such as Toulouse or Zaragoza. The data cannot prove long-range transport; however, air mass trajectory, MP transport and settling considerations suggest the MP emission sources to at least be regional (>100 km) given the population density within this local area. Longer-distance transport modelling may be possible but requires event-specific sampling and back-trajectory analysis to identify the extent of this transport. It is highly recommended that further monitoring and analysis be undertaken using separate dry and wet deposition sampling equipment. This would advance the understanding of the precipitation influence on atmospheric MP deposition and the wind trajectory impact on the quantity and composition of the atmospheric MP fallout.

Online content

Any methods, additional references, Nature Research reporting summaries, source data, statements of data availability and associated accession codes are available at https://doi.org/10.1038/s41561-019-0335-5.

Received: 26 July 2018; Accepted: 25 February 2019;
Published online: 15 April 2019

References

1. Rosevelt, C., Los Huertos, M., Garza, C. & Nevins, H. M. Marine debris in central California: quantifying type and abundance of beach litter in Monterey Bay, CA. *Mar. Pollut. Bull.* **71**, 299–306 (2013).
2. *Plastics—the Facts 2014/2015: an Analysis of European Plastics Production, Demand and Waste Data* (PlasticsEurope, 2015).
3. *Plastics—the Facts 2017: an Analysis of the European Plastics Production, Demand and Waste Data* (PlasticsEurope, 2017).
4. Song, Y. K. et al. Combined effects of UV exposure duration and mechanical abrasion on microplastic fragmentation by polymer type. *Environ. Sci. Technol.* **51**, 4368–4376 (2017).
5. da Costa, J. P. Micro- and nanoplastics in the environment: research and policymaking. *Curr. Opin. Environ. Sci. Health* **1**, 12–16 (2018).
6. Mattsson, K., Hansson, L.-A. & Cedervall, T. Nano-plastics in the aquatic environment. *Environ. Sci. Process. Impacts* **17**, 1712–1721 (2015).
7. Scheurer, M. & Bigalke, M. Microplastics in Swiss floodplain soils. *Environ. Sci. Technol.* **52**, 3591–3598 (2018).
8. Hurley, R., Woodward, J. & Rothwell, J. J. Microplastic contamination of river beds significantly reduced by catchment-wide flooding. *Nat. Geosci.* **11**, 251–257 (2018).

9. Gasperi, J. et al. Microplastics in air: are we breathing it in? *Curr. Opin. Environ. Sci. Health* **1**, 1–5 (2018).
10. Dris, R. et al. A first overview of textile fibers, including microplastics, in indoor and outdoor environments. *Environ. Pollut.* **221**, 453–458 (2017).
11. Dris, R., Gasperi, J., Saad, M., Mirande, C. & Tassin, B. Synthetic fibers in atmospheric fallout: a source of microplastics in the environment? *Mar. Pollut. Bull.* **104**, 290–293 (2016).
12. Cai, L. et al. Characteristic of microplastics in the atmospheric fallout from Dongguan city, China: preliminary research and first evidence. *Environ. Sci. Pollut. Res.* **24**, 24928–24935 (2017).
13. Corcoran, P. L. Environmental science processes and impacts benthic plastic debris in marine and fresh water environments. *Environ. Sci. Process. Impacts* **17**, 1363–1369 (2015).
14. Zbyszewski, M., Corcoran, P. L. & Hockin, A. Comparison of the distribution and degradation of plastic debris along shorelines of the Great Lakes, North America. *J. Great Lakes Res.* **40**, 288–299 (2014).
15. Zhang, K. et al. Microplastic pollution of lakeshore sediments from remote lakes in Tibet plateau, China. *Environ. Pollut.* **219**, 450–455 (2016).
16. Watkins, L., McGrattan, S., Sullivan, P. J. & Walter, M. T. The effect of dams on river transport of microplastic pollution. *Sci. Total Environ.* **664**, 834–840 (2019).
17. *Donnees Meteorologiques—Sud Ouest Bernadouze* (Centre d'Etudes Spatiales de la Biosphere, 2018); http://www.cesbio.ups-tlse.fr/data_meteo/index.php?perma=1319145390
18. *Demography* (Institut National de la Statistique et des Etudes Economiques, accessed 24 June 2018); https://www.insee.fr/fr/statistiques/3293086?geo=COM-09334
19. Araujo, C. F., Nolasco, M. M., Ribeiro, A. M. P. & Ribeiro-Claro, P. J. A. Identification of microplastics using Raman spectroscopy: latest developments and future prospects. *Water Res.* **142**, 426–440 (2018).
20. Zwaaftink, C. D. G. et al. Temporal and spatial variability of Icelandic dust emissions and atmospheric transport. *Atmos. Chem. Phys.* **17**, 10865–10878 (2017).
21. Camarero, L., Bacardit, M., de Diego, A. & Arana, G. Decadal trends in atmospheric deposition in a high elevation station: effects of climate and pollution on the long-range flux of metals and trace elements over SW Europe. *Atmos. Environ.* **167**, 542–552 (2017).
22. Marticorena, B. et al. Mineral dust over west and central Sahel: seasonal patterns of dry and wet deposition fluxes from a pluriannual sampling (2006–2012). *J. Geophys. Res. Atmos.* **122**, 1338–1364 (2017).
23. Morales-Baquero, R., Pulido-Villen, E. & Reche, I. Chemical signature of Saharan dust on dry and wet atmospheric deposition in the south-western Mediterranean region. *Tellus B* **1**, 1–12 (2013).
24. Schwikowski, M., Seibert, P., Baltensperger, U. & Gaggeler, H. W. A study of an outstanding Saharan dust event at the high-alpine site Jungfraujoch, Switzerland. *Atmos. Environ.* **29**, 1829–1842 (1995).
25. Dessens, J. & Van Dinh, P. Frequent Saharan dust outbreaks north of the Pyrenees: a sign of a climatic change? *Weather* **45**, 327–333 (1990).
26. van der Does, M., Knippertz, P., Zschenderlein, P., Giles Harrison, R. & Stuut, J.-B. W. The mysterious long-range transport of giant mineral dust particles. *Sci. Adv.* **4**, eaau2768 (2018).
27. Hidalgo-Ruz, V., Gutow, L., Thompson, R. C. & Thiel, M. Microplastics in the marine environment: a review of the methods used for identification and quantification. *Environ. Sci. Technol.* **46**, 3060–3075 (2012).
28. Norén, F. *Small Plastic Particles in Coastal Swedish Waters* (N-research, 2007).
29. Schindelin, J. et al. Fiji: an open-source platform for biological image analysis. *Nat. Methods* **9**, 676–682 (2012).
30. Erni-Cassola, G., Gibson, M. I., Thompson, R. C. & Christie-Oleza, J. A. Lost, but found with Nile Red: a novel method for detecting and quantifying small microplastics (1 mm to 20 µm) in environmental samples. *Environ. Sci. Technol.* **51**, 13641–13648 (2017).
31. Schymanski, D., Goldbeck, C., Humpf, H. U. & Fürst, P. Analysis of microplastics in water by micro-Raman spectroscopy: release of plastic particles from different packaging into mineral water. *Water Res.* **129**, 154–162 (2018).
32. *A European Strategy for Plastics in a Circular Economy* (European Commission, 2018).
33. Magnusson, K. et al. *Swedish Sources and Pathways for Microplastics to the Marine Environment: A Review of Existing Data* (IVL Swedish Environmental Research Institute Ltd, 2016).
34. Dris, R. et al. Beyond the ocean: contamination of freshwater ecosystems with (micro-) plastic particles. *Environ. Chem.* **12**, 539–550 (2015).
35. Shim, W. J., Hong, S. H. & Eo, S. in *Microplastic Contamination in Aquatic Environments* (ed. Zeng, E. Y.) 1–26 (Elsevier, Amsterdam, 2018).
36. Zender, C. S. Mineral Dust Entrainment and Deposition (DEAD) model: description and 1990s dust climatology. *J. Geophys. Res.* **108**, 4416 (2003).
37. Sanchez, E., Yague, C. & Gazetner, M. A. Planetary boundary layer energetics simulated from a regional climate model over Europe for present climate and climate change conditions. *Geophys. Res. Lett.* **34**, L01709 (2007).
38. Imhof, H. K. et al. Pigments and plastic in limnetic ecosystems: a qualitative and quantitative study on microparticles of different size classes. *Water Res.* **98**, 64–74 (2016).
39. Lenz, R., Enders, K., Stedmon, C. A., MacKenzie, D. M. A. & Nielsen, T. G. A critical assessment of visual identification of marine microplastic using Raman spectroscopy for analysis improvement. *Mar. Pollut. Bull.* **100**, 82–91 (2015).
40. Enders, K., Lenz, R., Stedmon, C. A. & Nielsen, T. G. Abundance, size and polymer composition of marine microplastics ≥10 µm in the Atlantic Ocean and their modelled vertical distribution. *Mar. Pollut. Bull.* **100**, 70–81 (2015).
41. Käppler, A. et al. Analysis of environmental microplastics by vibrational microspectroscopy: FTIR, Raman or both? *Anal. Bioanal. Chem.* **408**, 8377–8391 (2016).
42. Song, Y. K. et al. A comparison of microscopic and spectroscopic identification methods for analysis of microplastics in environmental samples. *Mar. Pollut. Bull.* **93**, 202–209 (2015).

Acknowledgements

The data were funded and provided by the CNRS TRAM Project, ANR-15-CE01-0008, Observatoire Homme-Milieu Pyrénées Haut Vicdessos—LABEX DRIIHM ANR-11-LABX0010 and CESBIO. The research leading to these results has also received funding from the People Programme (Marie Curie Actions) of the European Union's Seventh Framework Programme (FP7/2007-2013) under REA grant agreement no. PCOFUND-GA-2013-609102, through the PRESTIGE programme coordinated by Campus France. The authors acknowledge that this work was carried out in the CMAC National Facility, housed within the University of Strathclyde's Technology and Innovation Centre, who are funded with a UKRPIF (UK Research Partnership Institute Fund) capital award, SFC ref. H13054, from the Higher Education Funding Council for England (HEFCE).

Author contributions

S.A. and D.A. designed the study, undertook all the analyses and co-authored the manuscript. G.L.R. and V.R.P. provided the study design and analytical guidance and assisted in the preparation and revision of the manuscript. P.D. undertook all the field sampling and field protocol design, assisted in the sample preparation and contributed to the manuscript. A.S., S.B. and D.G. provided financial support and field site access that enabled this study to occur and contributed to the manuscript.

Competing interests

The authors declare no competing interests.

Additional information

Supplementary information is available for this paper at https://doi.org/10.1038/s41561-019-0335-5.

Reprints and permissions information is available at www.nature.com/reprints.

Correspondence and requests for materials should be addressed to D.A.

Publisher's note: Springer Nature remains neutral with regard to jurisdictional claims in published maps and institutional affiliations.

Methods

Field sampling and data collation. The field meteorology and sample station was visited five times over the five month monitoring period to acquire samples from the atmospheric fallout collectors. The sampling period extended from November 2017 to March 2018. Ideally, samples would be collected every four weeks, but because climatic conditions restricted access, the sample periods were inconsistent (sample durations of 12, 19, 34, 41 and 34 d, respectively, for samples from November to March). Field blanks were also collected. During this period two independent atmospheric deposition collectors were active at the site. The first collector was a Palmex Rain Sampler with a sampling area of 0.014 m^2 (diameter of 135 mm) (constructed of ultraviolet-resistant polyvinyl chloride (PVC) and stainless steel). The second collector installed and sampled from was a NILU Particulate Fallout Collector (p.no. 9721) with a sampling area of 0.03 m^2 (diameter 200 mm) (constructed of high-density PE and stainless steel). Both collectors were open to the atmosphere for the total period of sampling and therefore all the samples are a combination of dry and wet atmospheric fallout. The samples collected from each atmospheric fallout collector were kept separate (both during the field sampling and the laboratory sample preparation) and thus provide a duplicate sample data set for each monitoring period.

During the collection of the sample material (and at all times when near the sampler), all the personnel were careful to remain downwind of the sampler, samples exposure time was kept to a minimum and, whenever possible, cotton clothing was worn to minimize contamination. The total sample volume was collected (without subsampling). Samples from the Palmex collector were decanted into clean glass 2 litre bottles in the field, capped and transported back to the laboratory. The field sample container from the NILU collector was capped and transported back to the laboratory where samples were decanted into clean glass 2 litre bottles in the laboratory 'clean room'. All the decanted samples were stored in a dark walk-in refrigerator (at 4 °C) until filtration and sample processing commenced.

In conjunction with physical atmospheric samples, wind, humidity, temperature, rainfall and snowfall data were recorded at the monitoring site by the CESBIO (Centre d'Etudes Spatiales de la Biosphere) meteorological gauging station[17]. This data set provided local microclimate information at a 30 minute timestep.

Sample processing preparation for MP analysis. All samples (2 × 5 field samples) contained varying amounts of organic and inorganic matter, which include biofilm and dust. To aid the analysis, it is necessary to remove as much of the biogenic and non-plastic inorganic material as possible without damaging or losing potential plastic particles. It is also necessary to remove biofilm from the plastic prior to micro-Raman spectroscopy to ensure an effective analysis (spectra clarity). To this end, protocols were selected with the minimum physical manipulation, least number of steps and the least-aggressive digestion chemicals and temperatures possible to achieve the desired results. Sample material was filtered through a 0.45 µm polytetrafluoroethylene 47 mm diameter membrane (Whatman) using borosilicate laboratory glass filtration equipment and then vacuum dried with ethanol (96 vol%). Filters were examined and photographed under a stereomicroscope Olympus SZX10 with an Olympus SC30 camera attachment (and visually checked using an Axiostar Plus (×50) microscope) to record as much detail of the potential plastic particles as possible prior to digestion. The filter was then rinsed into borosilicate glass test tubes with 10 ml of hydrogen peroxide (H_2O_2) solution 30%, capped with glass stoppers and placed in a static heat block (Thermomix) at 55 °C for 7 d (no agitation). On day 8 a further 5 ml of H_2O_2 solution 30% w/w was added to each sample and the sample was left for a further 7 d. H_2O_2 was chosen as the digestion medium because it was used in previous studies[7,30,43,44], but given the low usage temperature of some plastics (PS = 70 °C and PVC = 60 °C)[45] and the risk of glassing or melting at elevated temperatures, the temperature was purposefully maintained below 60 °C to ensure the methodology did not affect the characterization or result in the loss of material.

On day 14 the sample was filtered onto a 0.45 µm polytetrafluoroethylene 47 mm diameter filter membrane, rinsed with 250 ml MilliQ (18 MΩ cm) water and dried with ethanol (96 vol%). The filtered material was then rinsed into density separation glassware with zinc chloride (Technipur $ZnCl_2$) at a 1.6 g ml^{-1} density. This was gently agitated (60 revolutions per minute) for 7 d at room temperature (Edmund Buhler KS-15 shaker). the settled material was drained away with the sediment removal valve and the remaining sample filtered onto 0.2 µm, 25 mm diameter aluminium oxide filters (Anodisc 25). Glassware was triple rinsed onto the filter with a pH 4 buffer. The filter was then rinsed with 250 ml MilliQ water and vacuum dried with ethanol. The resulting filter was then examined and photographed again to look for changes in either the number of particles or particle character. Although it is difficult to quantify particles predigestion (due to excessive organic/inorganic material) many of the particles photographed previously were identifiable and any visible change in the material was noted, and thus we are confident that the protocols were sufficiently gentle to ensure minimal losses of material.

Blank test. Two sets of laboratory blanks were created in support of this sample preparation process. Two MilliQ samples of 1 litre, instead of field sample material, were put through the full digestion and zinc chloride separation process, which resulted in two full-process blanks (following in detail the process outlined for the sample preparation).

A further two laboratory blanks (MilliQ water samples) underwent the digestion process, but were filtered onto the Anodisc 25 filters without zinc chloride separation. The purpose of these blanks was to help quantify the possible MP contamination caused by the sampling and sample preparation process.

Field blanks were also collected from each collector. Sample collection containers (glass) were taken out on site, connected to and opened at the sample location and then returned to the laboratory. These 'empty' glass containers were then thoroughly rinsed with MilliQ water and the resulting water processed without the zinc chloride separation, following the preparation described above.

The blank test resulted in a total of six blank samples, two from the complete preparation and $ZnCl_2$ process and four without $ZnCl_2$ separation. The blank filters identified, on average, 3 ± 1 fibres, 1 ± 1 film and 8 ± 1 fragments per filter.

Visual and ImageJ/Fiji particle inspection and count. All filters were visually inspected under a stereo microscope for MP particles using the identification criteria published by Hidalgo-Ruz et al.[27], Löder and Gerdts[46], and Norén[28]. Noted that to use visual identification alone is not recommended for MP <500 µm, and so a second technique (Fourier transform infrared and Raman spectroscopy) is recommended to confirm small particles[27,28,46,47]. Plastic particulates are visually identified by their shape and colour. Plastics must have no biogenic (cellular) structure; fibres are expected to have a relatively even or consistent thickness along the fibre length and illustrate three dimensional bending; fragments and films are expected to have relatively homogeneous colouring and illustrate a level of transparency or clarity[28,46]. Aged plastic, such as expected in environmental samples, is described by Hidalgo-Ruz et al.[27] to present embrittled and weathered surfaces, and to have irregular shapes with broken and sharp edges. Weathered plastics may also show pitting. Colour is also a plastic identifier[27,46] and ranges from transparent and variations of white to bright orange, blues, greens and purples through to black. It is noted that biogenic material becomes bleached during the sample preparation process (H_2O_2 digestion) that makes plastic particulates with colour highly visible and differentiated from residual (postdigestion) biogenic material.

An initial, indicative fragment, fibre and film count was visually undertaken for each sample using an Olympus SZX10 stereomicroscope. Three locations of 13 mm^2 were randomly selected and investigated on each filter (two filters per sample, with random selection to minimize bias)[48]. After the visual identification methodology, a count of plastic fragments, fibres and films was undertaken (n = 6 inspected areas for each sample, with a total of 254 MPs identified). The identification was conservative with a focus on obvious coloured particulates, which resulted in a possible overall under-estimation due to the limited count or testing of white and non-transparent materials.

All the filters were then photographed using a Leica DM6000M confocal microscope with a Marzhauser Scan 130 × 85 4 mm X–Y motorized stage. Photographs were manually focused for each frame using a ×10 lens. Filters were photographed using the automated mosaic software (Leica proprietary software) and automatically stitched to provide a multistep mosaic image for each filter. The visual count was repeated on the photographs and completed using the software ImageJ. Three 13 mm^2 photographed areas of each filter were imported into ImageJ. Particle counts were undertaken using the protocol defined and used by Erni-Cassola et al.[30] (ImageJ code provided in the supplementary material of Erni-Cassola et al.[30]). A second count was undertaken following the same method using a larger area (6 × 58 mm^2) to provide a visual/ImageJ MP count for 50% of the Anodisc 25 filter surface. All the identified particles (n = 1,147) were sized using ImageJ (as completed in Isobe et al.[49] and Imhof et al.[38]) to provide a length, width and area appropriate for PSD analysis.

Raman set-up and analysis. Confirmation of the presence and type of plastic was achieved by a micro-Raman (Horiba Scientific Xplora Plus, 50–3,200 cm^{-1} with a 1.5 cm^{-1} resolution and confocal imaging accuracy of 0.5 µm) confocal microscope with a motorized X–Y stage. Micro-Raman spectroscopy was used in previous studies to confirm visual and Nile Red fluorescence-assisted MP quantification in environmental samples[30,41,39–42] and has been shown to be effective in MP characterization down to 1 µm (ref. [19]). Three areas of each filter (6 × 13 mm^2) were randomly selected and analysed for the total plastic presence using the 785 nm laser (spatial resolution of 1 µm) and 200–2,000 cm^{-1} Raman shift range. Spectra were collected using an acquisition time of 15 s and ten accumulations at a maximum of 25% power (filter) (general settings: 1,200 gratings mm^{-1} with a 50 µm split, modified to achieve effective spectra results as necessary during the analysis). Laser power settings were tested on plastic particles to establish the strength necessary for effective spectra imaging with the minimal particulate damage. A laser power of 25% resulted in no visible damage to the plastics and an acceptable spectra delineation. Laser powers of 50% and 100% resulted in damage (burning or melting) of the plastic, as shown in the Supplementary Note 4.

Each suspected plastic particle was analysed individually, which resulted in a data set of Raman shift spectra (n = 245 particulates). Each potential identified MP was analysed twice (at two unique locations on the particle) to confirm the

Raman spectra. Where the spectra were unclear or not definitive, a third analysis was undertaken. Samples that illustrated three unclear spectra were defined as 'not plastic'. The blank filters were tested to quantify the level of contamination (through sample processing and analysis). A new Anodisc 25 filter was also analysed to confirm the background filter spectra. The micro-Raman spectral analysis provided confirmation of the visual identification, which supports the extrapolation of visual counts to consider spatial and temporal trends.

Raman spectra analysis. Open source Spectragryph software and databases[50] were used to analyse the micro-Raman spectral results. An individual evaluation of each spectrum was completed, similar to methods of spectral analysis followed in Lenz et al.[45], Khashaba et al.[51] and Ševčík and Mácová[52] in conjunction with Lagaron et al.[53], to provide a clear definition of the chemical and bond spectra peaks.

Statistical analysis. Visual and ImageJ MP counts of all the filters were confirmed using micro-Raman spectrography (11% of the filters were analysed using micro-Raman and 50% of the filters were inspected visually and with ImageJ). The micro-Raman confirmed count of MP mm^{-2} was extrapolated to provide an indication of the quantity of MPs per filter and therefore per sample. It is acknowledged that extrapolation from subsampled filters does not provide a definitive MP count and ideally all MP particulates would be counted and confirmed with micro-Raman analysis. Due to analysis constraints, a complete filter analysis was not possible.

The calculation of MP $m^{-2}\,d^{-1}$ was calculated through a simple sum of sample area MP counts, scaling using known filter and collector areas and known monitoring period durations. The calculations used the following simple equations:

$$\overline{X} = \frac{\left(\sum X_{1-n}\right)}{n} \quad (1)$$

$\overline{X}$ = the average MP count for a sample area (13 mm^2), $X_{1,2,3}$ = the MP count for a sample area 1, 2, 3, etc. (sample area = 13 mm^2) and n = sample area number (six sample areas were investigated for each sample period).

$$\mu P = \left(\overline{X} \times \frac{Y}{y}\right) - \varepsilon \quad (2)$$

where μP = the total MP count per filter, y = the sample area (13 mm^2 or 0.000013 m^2), Y = the total filter area (346 mm^2 or 0.0003 m^2) and ε = the sampling error, the number of MP particulates found on the blank samples.

$$MP = \left(\mu P \times \frac{1}{a}\right)/d \quad (3)$$

where MP = MP count $m^{-2}\,d^{-1}$, a = the sample area of the atmospheric collector (m^2) and d = duration of the sampling period (days).

The quantity of MPs per filter is accepted to be representative of the atmospheric deposition for the monitoring period relative to the collection area (Palmex collector = 0.014 m^2, NILU collector = 0.03 m^2). The provision of MP quantity per square metre has been previously published and accepted as a method that supports the comparison of the results of multiple studies[8]. Therefore, the results per monitoring period were normalized for time period of 1 d (for comparison with Dris et al.[11] and Cai et al.[12]) and a 1 m^2 area using the known collector surface areas. The two collectors provide replicate samples for each sample period and therefore were treated as such. Thus, two independent samples were collected for each sample period, which provided two Anodisc 25 filters, with a total of six randomly selected areas analysed for MPs and resulted in $n = 6$ per monitoring period.

Statistical analysis of the MP counts and characteristics were purposefully kept to a minimum due to the data set duration (five monitoring periods) and the constraints of a single site case study (it is not considered appropriate to generalize from a single case study, so the study is presented as a first indication and presentation of remote MP presence only). Simple correlation analysis between the particle counts and meteorological data was completed using R Studio (R version 3.4.1) software and standard significance (P value), and Pearson and Spearman correlation tests appropriate to the data (CRAN packages hydroGOF, Hmisc, Performance Analytics and subsidiaries) were used .

Bias. Use of a non-automated system in particle counting and analysis induces a level of human bias in the results. To reduce the potential human bias in the results due to the lack of automation, random sampling was employed for all filter counting and micro-Raman analysis site selection. MP visual, ImageJ and micro-Raman analysis was undertaken in triplicate on all filters to further limit bias and uncertainty in the results. MP identification was completed following an identification protocol that was consistently employed on all the areas analysed. The identification protocol was conservative; any particles that did not meet the visual identification protocol as described by Hidalgo-Ruz et al.[27] and Norén[28] and/or did not provide a clear Raman plastic signature were discounted from the analysis to limit misidentification and bias.

Local transport trajectory and source area assessment. The recorded wind, rain and snow meteorological data were used to support a local MP transport assessment and to help consider potential source and trajectories of MP particles relative to the field site. The simple numerical assessment of distance and transport duration of MP particles relative to rainfall events, snowfall events and wind occurrences (events) were calculated using the known field site elevation, upper elevation of MP entrainment[37], wind speed and assumed settling velocity[36] (based on a 25 µm dust particle). Once elevated, it was assumed that no further meteorological updraft or conveyance assistance (other than the recorded horizontal wind speed and direction) influenced the MP (to provide a simplified assessment of possible MP transport):

$$\text{Distance} = \text{back-trajectory duration}/\text{wind speed} \quad (4)$$

where distance = the potential horizontal trajectory of MP (m), back-trajectory duration = the duration the MP is airborne (s) calculated as the maximum elevation (600 m a.g.l.)/settling velocity (0.1 m s^{-1}) (refs. [36,37]), and wind speed = the maximum recorded wind speed (at the meteorological station) during each rain, snow or wind event (m s^{-1}).

The wind directions recorded for the rain, snow and wind events were used in conjunction with the calculated horizontal transport distances to create event-specific wind rose maps to spatially illustrate the local MP trajectories. It is acknowledged that this is a highly simplified assessment of the potential horizontal transport trajectories and does not take into account the complex atmospheric dynamics of mountain terrain or atmospheric mixing. However, it does provide a first simplified assessment of local MP transport.

HYSPLIT4 analysis. The open source modelling software HYSPLIT4[54,55] was used to model the back trajectory of air parcel movement from the field site during the five monitoring periods. HYSPLIT4 was used to download and model global wind and/atmospheric meteorology data provided by the National Oceanic and Atmospheric Administration (Global Data Assimilation System data) (similarly used in Su et al.[56], Ashrafi et al.[57] and Reche et al.[58]). Each rainfall ($n = 165$), snowfall ($n = 186$) and wind event >2 m s^{-1} ($n = 197$) was individually modelled with the back-trajectory duration defined as in equation (4). The multiple individual trajectories were then collated to create a frequency chart of trajectory potentials across the local area. The source point (deposition location in a back-trajectory model) was set to 43° N 1° E and 100 m a.g.l.

Data availability

The authors confirm that all the data that underlie the results presented in this study are available within the Supplementary Information files and can be downloaded in conjunction with this paper.

References

43. Digka, N., Tsangaris, C., Kaberi, H., Adamopoulou, A. & Zeri C. *Proc. Int. Conf. Microplastic Pollution Mediterranean Sea* (eds Cocca, M., Di Pace, E., Errico, M. E., Gentile, G. & Montarsolo, A.) 17–24 (Springer, Cham, 2018).
44. Wang, W., Ndungu, A. W., Li, Z. & Wang, J. Microplastics pollution in inland freshwaters of China: a case study in urban surface waters of Wuhan, China. *Sci. Total Environ.* **575**, 1369–1374 (2017).
45. Klein, R. *Laser Welding of Plastics: Materials, Processes and Industrial Applications* 3–69 (John Wiley & Sons, Weinheim, 2012).
46. Löder, M. & Gerdts, G. in *Marine Anthropogenic Litter* (eds Bergmann, M., Gutow, L. & Klages, M.) (Springer, Cham, 2015).
47. Shim, W. J., Hong, S. H. & Eo, S. E. Identification methods in microplastic analysis: a review. *Anal. Methods* **9**, 1384–1391 (2017).
48. Peeken, I. et al. Arctic sea ice is an important temporal sink and means of transport for microplastic. *Nat. Commun.* **9**, 1–9 (2018).
49. Isobe, A., Uchida, K., Tokai, T. & Iwasaki, S. East Asian seas: a hot spot of pelagic microplastics. *Mar. Pollut. Bull.* **101**, 618–623 (2015).
50. Menges, F. *Spectragryph—Optical Imaging Software* (2016); https://www.effemm2.de/spectragryph/
51. Khashaba, P. Y., Ali, H. R. H. & El-Wekil, M. M. A rapid Fourier transform infrared spectroscopic method for analysis of certain proton pump inhibitors in binary and ternary mixtures. *Spectrochim. Acta A* **190**, 10–14 (2018).
52. Ševčík, R. & Mácová, P. Localized quantification of anhydrous calcium carbonate polymorphs using micro-Raman spectroscopy. *Vib. Spectrosc.* **95**, 1–6 (2018).
53. Lagaron, J. M., Dixon, N. M., Reed, W., Pastor, J. M. & Kip, B. J. Morphological characterisation of the crystalline structure of cold-drawn HDPE used as a model material for the environmental stress cracking (ESC) phenomenon. *Polymer* **40**, 2569–2586 (1999).
54. Draxler, R. R. & Hess, G. D. *Description of the HYSPLIT4 Modelling System.* NOAA Technical Memorandum ERL ARL-224 (Air Resources Laboratory, 2018); https://www.researchgate.net/publication/255682850_Description_of_the_HYSPLIT_4_modelling_system

55. Stein, A. et al. NOAA's HYSPLIT atmospheric transport and dispersion modeling system. *Bull. Am. Meteorol. Soc.* **96**, 2059–2077 (2015).
56. Su, L., Yuan, Z., Fung, J. C. H. & Lau, A. K. H. A comparison of HYSPLIT backward trajectories generated from two GDAS datasets. *Sci. Total Environ.* **506–507**, 527–537 (2015).
57. Ashrafi, K., Shafiepour-Motlagh, M., Aslemand, A. & Ghader, S. Dust storm simulation over Iran using HYSPLIT. *J. Environ. Health Sci. Eng.* **12**, 9 (2014).
58. Reche, I., D'Orta, G., Mladenov, N,. Winget, D. M. & Suttle, C. A. Deposition rates of viruses and bacteria above the atmospheric boundary layer. *ISME J.* **12**, 1154–1162 (2018).